

Secondary Guest-Driven Nucleation of N₂O Clathrate Hydrate in Amorphous Ice Mixture under Ultrahigh Vacuum

Bijesh K. Malla,[‡] Soham Chowdhury,[‡] Samir Kumar Nayak, Sofia Sara Baji, Teena J Mathew, Rabin Rajan J Methikkalam, Sharma S. R. K. C. Yamijala,^{*} Rajnish Kumar,^{*} and Thalappil Pradeep^{*}



Cite This: *J. Phys. Chem. Lett.* 2025, 16, 12720–12727



Read Online

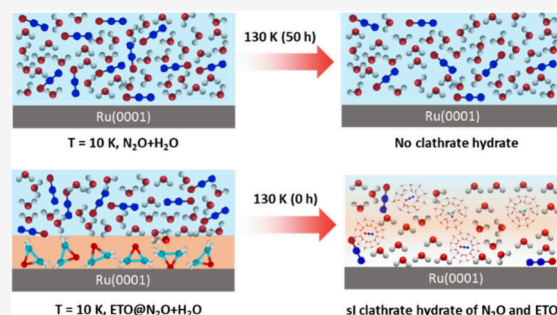
ACCESS |

Metrics & More

Article Recommendations

Supporting Information

ABSTRACT: We report the first observation of nitrous oxide (N₂O) clathrate hydrate (CH) under ultrahigh vacuum (UHV) conditions using infrared spectroscopy. While nucleation of CHs from water and guest molecules either spontaneously or in the presence of promoters is well-established under high-pressure conditions, their occurrence under cryogenic UHV remains less understood, particularly in multiguest systems. In this study, binary and ternary ice mixtures of N₂O, ethylene oxide (ETO), dimethyl ether (DME), tetrahydrofuran (THF), and H₂O were investigated via thermal annealing at 130 K. The binary N₂O–H₂O system showed no signs of hydrate formation after 50 h of annealing, whereas the addition of ETO, DME, or THF led to immediate CH formation under identical conditions. This demonstrates a clear promoter-assisted heterogeneous nucleation mechanism. In situ reflection absorption infrared (RAIR) spectroscopy confirms that ETO facilitates the formation of structure I hydrates, incorporating both ETO and N₂O in the cages, while DME and THF promote larger-cage CHs. Density functional theory calculations support experimental RAIR results, which predict stronger host–guest interactions and blue shifts for small cages and weaker shifts for large cages. These findings offer new mechanistic insights into multiguest hydrate nucleation and establish N₂O CH formation under UHV as a relevant process in cryogenic and astrochemical environments.



Nitrous oxide (N₂O) is a potent greenhouse gas with a global warming potential approximately 300 times greater than that of carbon dioxide (CO₂) over a 100-year time scale.¹ Beyond its climatic impact, N₂O contributes to stratospheric ozone depletion through photodissociation.² According to the U.S. Environmental Protection Agency (EPA), anthropogenic sources accounted for about 5% of total greenhouse gas emissions in the United States in 2013.³ Interestingly, N₂O is not confined to Earth; it has also been detected in interstellar regions such as Orion KL and Sagittarius B2, indicating that nitrogen–oxygen bond formation occurs under extreme conditions of the interstellar medium (ISM).^{4,5} Recent observations from the James Webb Space Telescope (JWST) suggest the presence of condensed-phase N₂O in protostellar environments, further underscoring its astrochemical relevance.⁶

Considering the presence of N₂O in terrestrial and astrophysical environments, understanding its potential for physical trapping and chemical transformation in icy matrices is of significant interest. One mechanism by which volatile molecules such as N₂O may be sequestered is through clathrate hydrates (CHs). CHs are crystalline solids made of hydrogen-bonded water molecules that form polyhedral cages that encapsulate guest species such as CH₄, CO₂, ethane, etc.^{7,8} These structures, which typically adopt structure I (sI), structure II (sII), or structure H (sH), naturally form under

high-pressure and low-temperature conditions found in deep ocean sediments and planetary ices.^{9,10} CHs are believed to play a major role in cometary outgassing events. The observed outgassing patterns in the Northern Hemisphere suggest that comet 67P's nucleus contains a combination of crystalline ice, CHs, and other ices, contradicting the hypothesis that its volatiles were primarily trapped in an amorphous ice phase.¹¹ Recent laboratory experiments have demonstrated that CHs can also form under UHV and cryogenic conditions, broadening the potential relevance of CHs to astrophysical ices.^{12–14} For instance, thin-film clathrates of THF have been successfully synthesized and structurally confirmed via electron diffraction.¹⁵

Despite growing evidence for clathrate formation under nontraditional conditions, the fundamental process of nucleation remains poorly understood. Classical nucleation theory (CNT) suggests that hydrate formation begins once a critical cluster of host and guest molecules is formed.¹⁶ In

Received: September 8, 2025

Revised: November 18, 2025

Accepted: November 24, 2025

Published: December 5, 2025



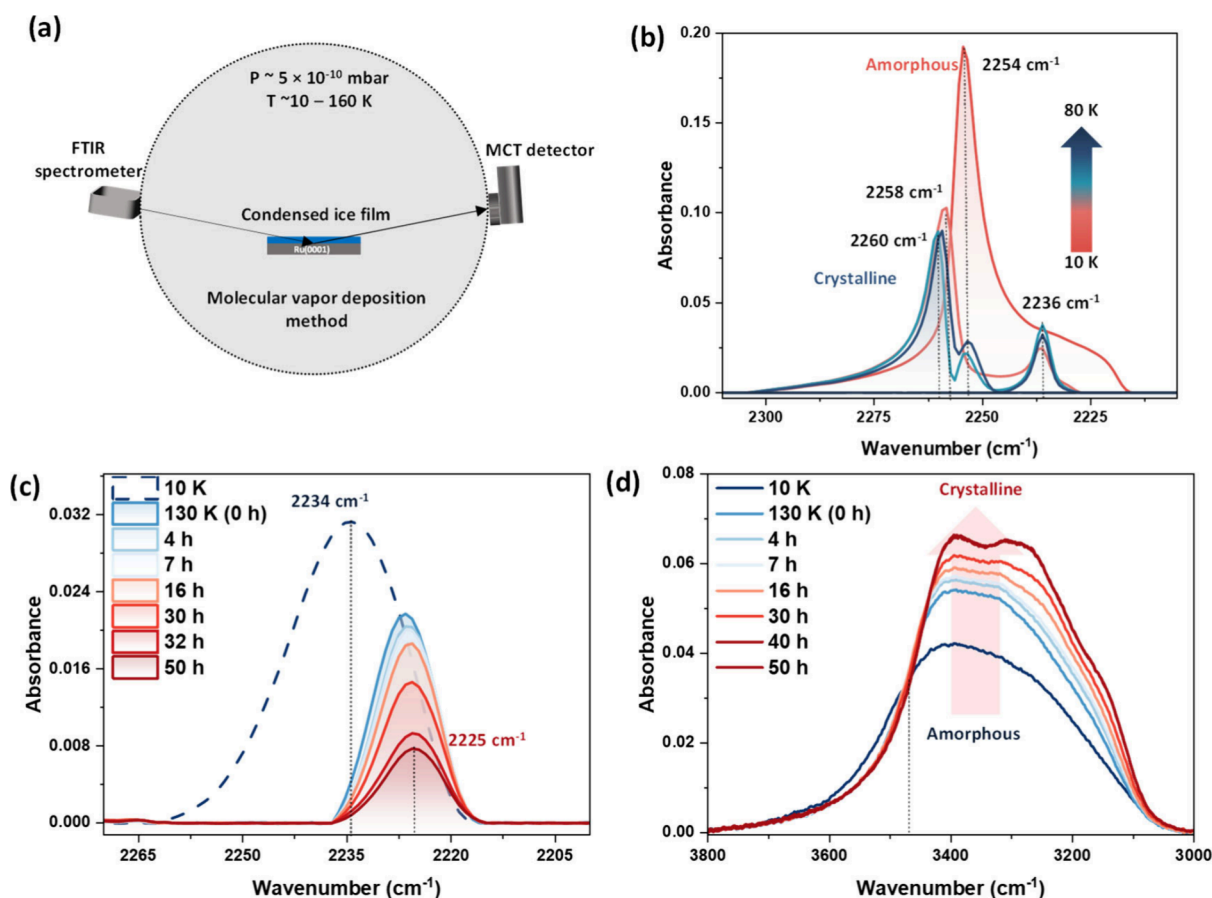


Figure 1. (a) A simplified schematic of the UHV instrument used for this work. (b) Temperature-dependent RAIR spectra of 150 ML of N_2O ice in the N–N–O asymmetric stretching region. Temperature- and time-dependent RAIR spectra of 300 ML of N_2O + H_2O ice in the N–N–O asymmetric stretching region (c) and in the O–H stretching region (d).

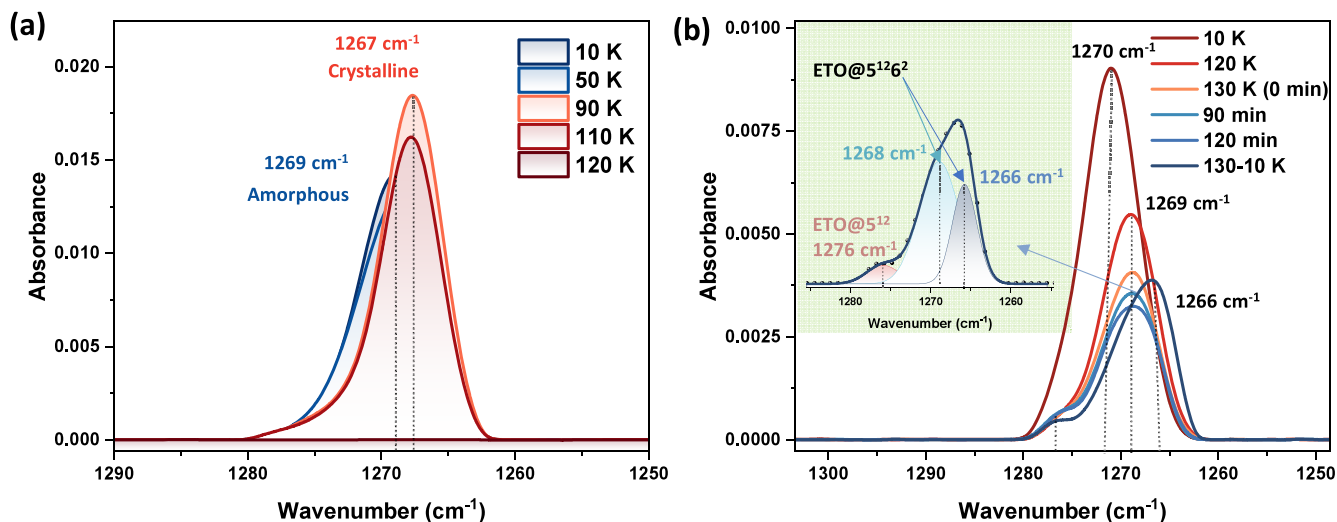


Figure 2. (a) Temperature-dependent RAIR spectra of ETO ice in the ring-breathing region. (b) RAIR spectra of ETO + H_2O ice in the ring-breathing region. The spectrum, acquired after annealing at 130 K for 2 h and subsequently cooling to 10 K, is deconvoluted into three distinct peaks located at 1276 cm^{-1} (red), 1268 cm^{-1} (sky blue), and 1266 cm^{-1} (blue).

contrast, simulations propose a two-step mechanism involving the formation of an amorphous precursor that later crystallizes into a stable hydrate structure.^{17,18} Our prior work using amorphous mixtures of water and various guest molecules under UHV revealed that most CHs formed under these conditions are metastable,¹⁹ often reverting to cubic or

hexagonal ice.^{20–22} Among the systems tested, only tetrahydrofuran (THF, $\text{C}_4\text{H}_8\text{O}$) consistently formed stable CHs, and these findings were attributed primarily to homogeneous nucleation processes.^{15,23}

Building upon these observations, we turned our attention to N_2O , a known sI clathrate former under high-pressure

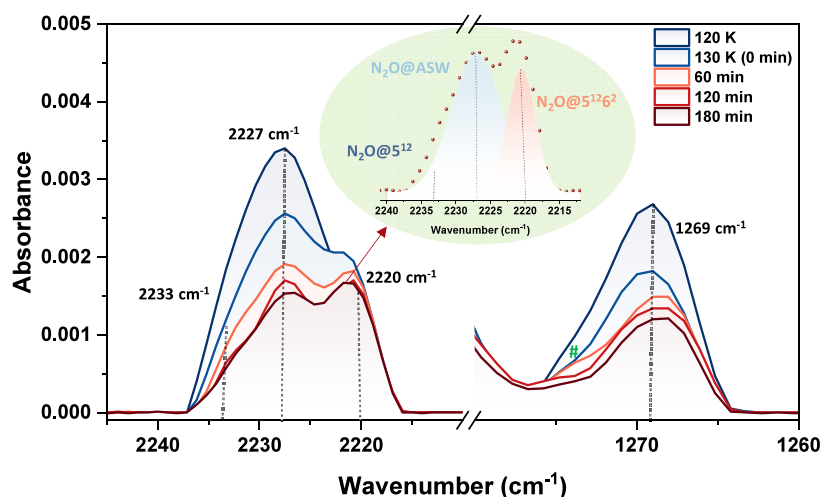


Figure 3. RAIR spectra of ETO@N₂O + H₂O showing the N–N–O asymmetric stretching region of N₂O and the ring-breathing mode of ETO. After 180 min, the N–N–O stretching band is deconvoluted into three components, with peaks centered at 2233 cm⁻¹ (deep blue), 2227 cm⁻¹ (light blue), and 2220 cm⁻¹ (red). The peak labeled as # in the spectra in the ring breathing mode is attributed to the ETO occupied in the small cage.

Table 1. Calculated Infrared Frequencies of N₂O and ETO in the N–N–O Asymmetric Stretching Region and the Ring-Breathing Region

System	N ₂ O	N ₂ O@5 ¹²	N ₂ O@5 ¹² 6 ²	N ₂ O@5 ¹² 6 ⁴
Frequency (cm ⁻¹)	2267.93	2286.69	2272.89	2269.74
System	ETO	ETO@5 ¹²	ETO@5 ¹² 6 ²	ETO@5 ¹² 6 ⁴
Frequency (cm ⁻¹)	1257.19	1272.19	1262.70	1259.17

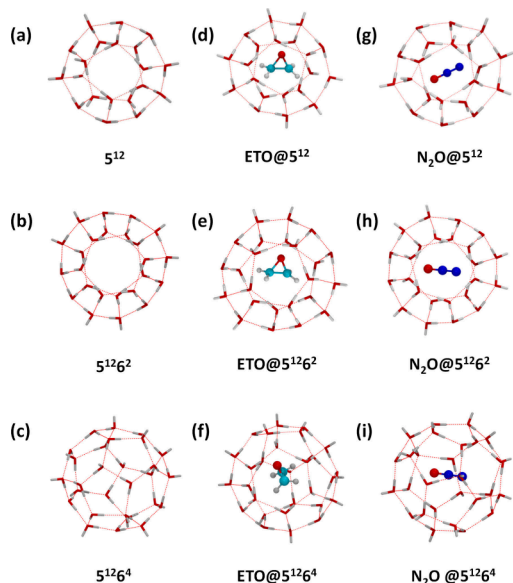


Figure 4. Optimized geometries of (a–c) empty 5¹², 5¹²6², and 5¹²6⁴ CH cages; (d–f) ETO inside the 5¹², 5¹²6², and 5¹²6⁴ CH cages; (g–i) nitrous oxide encaged in the 5¹², 5¹²6², and 5¹²6⁴ CH cages.

conditions, as supported by X-ray diffraction and Raman data.^{24–26} We aimed to investigate whether N₂O could form CHs from amorphous N₂O–H₂O ice mixtures under UHV and cryogenic conditions, which more closely resemble interstellar ice environments.⁶ Surprisingly, N₂O alone failed to nucleate a clathrate phase in contrast to other guest molecules. To address this, we introduced ethylene oxide

(ETO/C₂H₄O), a molecule previously shown to nucleate sl CHs under vacuum conditions, as a coguest.^{27–29} Remarkably, as ETO initiated CH formation, N₂O got incorporated into the clathrate lattice, suggesting a conucleation mechanism or surface-mediated heterogeneous nucleation. This mechanism is further supported by additional experiments involving other known hydrate formers such as THF and dimethyl ether (DME/C₂H₆O).

This work presents the first IR spectroscopic evidence of the existence of N₂O CH under UHV conditions. The ability of N₂O to form mixed CHs with ETO extends the known range of CH-forming systems and offers important implications for astrochemistry. In particular, such mixed ices could serve as precursors for complex organic molecules, including amino acids and nucleobases, when exposed to ionizing radiation in space.³⁰ This study provides new insights into the physical chemistry of clathrate nucleation and potential pathways for molecular evolution in icy astrophysical environments.

All experiments were conducted using a custom-built ultrahigh vacuum (UHV) chamber, as described in detail in our previous study (Figure 1a).³¹ Thin ice films of N₂O, H₂O, ETO, DME, and THF were prepared by background vapor deposition. The ice thickness was estimated based on the ion gauge sensitivity factor, deposition time, and background pressure. Quantum chemical calculations for free and encapsulated N₂O and ETO were performed using the B3LYP³² functional with the 6-311++G(d,p)³³ basis set. Additional methodological details are provided in the Supporting Information.

At the outset, 150 ML of N₂O ice were deposited on a Ru(0001) substrate at 10 K. Figure 1b and Figure S1 present the temperature-dependent RAIR spectra of the deposited N₂O ice in the N–N–O asymmetric and symmetric stretching region. At 10 K, a sharp peak at 2254 cm⁻¹ and a broad feature in the lower wavenumber region (2245–2215 cm⁻¹) were observed, indicating that the N₂O ice is in an amorphous state. Since N₂O is structurally similar to CO₂, it exhibits two distinct peaks for the ν₃ stretching mode, corresponding to the transverse optical (TO) and longitudinal optical (LO) modes. The higher wavenumber feature (2254 cm⁻¹) corresponds to the LO mode, while the lower wavenumber broad peak

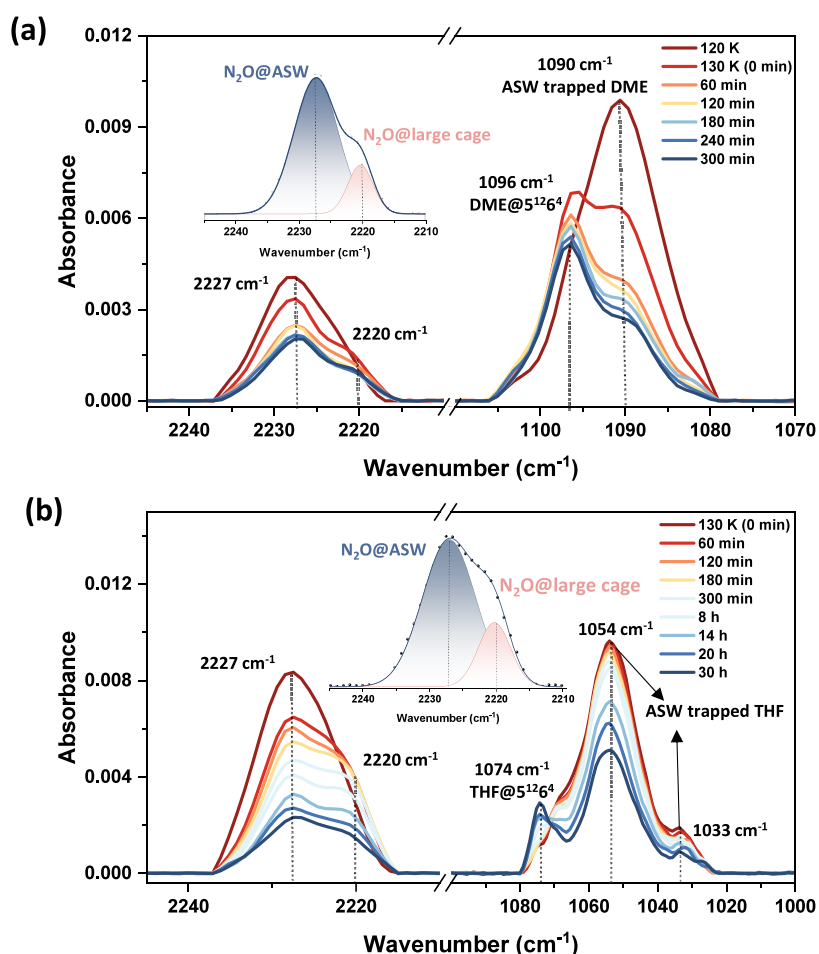


Figure 5. (a) RAIR spectra of DME@N₂O + H₂O in the N–N–O asymmetric stretching region of N₂O and the C–O–C asymmetric stretching region of DME. After 300 min, the N–N–O stretching band is deconvoluted into two components, centered at 2227 cm⁻¹ (highlighted in deep blue) and 2220 cm⁻¹ (highlighted in red). (b) RAIR spectra of THF@N₂O + H₂O in the N–N–O asymmetric stretching region of N₂O and the C–O asymmetric stretching region of THF. Similarly, the spectrum after 300 min shows the N–N–O stretching band resolved into two components at 2227 cm⁻¹ (deep blue) and 2220 cm⁻¹ (red).

represents the TO mode.^{34–37} The RAIRS measurement was performed at a grazing incidence angle of 82.75°,³¹ which enhances the contribution from the LO mode, thus explaining the higher intensity of the 2254 cm⁻¹ peak. We note that the experiments were performed on a Ru metal surface, where the surface dipole selection rule suppresses the TO mode, thereby making the LO mode more prominent.³⁸ Consistent with this substrate dependence, Cassidy et al.³⁹ reported two distinct infrared spectra for the N–N–O asymmetric stretch of N₂O on silica versus Cu: the silica support retains TO activity, whereas the metallic Cu surface, subject to the same selection rule as Ru, leads to an LO-dominated profile.³⁹

Upon annealing the N₂O ice to its desorption temperature (~80 K), the amorphous ice undergoes crystallization, likely forming cubic crystalline ice in two stages.^{40,41} During this process, the 2254 cm⁻¹ peak splits into two components (2258 and 2254 cm⁻¹), and its intensity decreases. The broad peak also sharpens, evolving into a distinct peak at 2236 cm⁻¹. This decrease in intensity is attributed to dipole alignment during crystallization, which reduces the dipole moment fluctuations and hence the infrared absorption. Similar behavior has been previously reported using various spectroscopic techniques.^{42,43} In the symmetric stretching region (Figure S1), a broad peak at 1296 cm⁻¹ indicates the amorphous phase and a

sharp peak at 1299 cm⁻¹ indicates the crystalline phase. We note here that 150 ML of N₂O ice RAIR spectra are also given in our earlier paper,⁴⁴ Supporting Information, but a detailed analysis of spectral features has not been done.

To investigate the formation of N₂O CH, 300 ML of a N₂O:H₂O ice mixture in a 1:5 ratio was codeposited and thermally annealed to 130 K, where it was held for 50 h. During the initial warming from 10 to 130 K, a red shift was observed, accompanied by a decrease in the peak intensity of the N–N–O asymmetric stretch (Figure 1c, Figure S2), which is attributed to the desorption of N₂O from the ice matrix. Upon annealing at 130 K, the band intensity decreases with no further frequency change, indicating no new interaction, only a declining N₂O/H₂O ratio. Thus, once the frequency stabilizes, the number of H₂O molecules coordinated to N₂O appears to be constant. Additionally, in the symmetric stretching region, the same trend was observed, where we only saw a decrease in the peak position at 1299 cm⁻¹ (Figure S3). We note here that the available data do not allow us to distinguish specific N₂O–H₂O conformations, so we refrain from making a conformer assignment. Additional temperature-dependent experiments with 1:10 and 1:20 of N₂O:H₂O (Figure S4) ratios showed similar behavior, peak red-shifting and decreasing intensity, likely due to enhanced hydrogen bonding between the N₂O

and surrounding water molecules.³⁵ Unlike our earlier work, N₂O does not exhibit facile homogeneous nucleation of CHs. In the O–H stretching region (Figure 1d), sharpening of the peaks was observed, consistent with the formation of crystalline water ice.⁴⁵ At low N₂O concentrations in H₂O ice, the O–H stretching region is only weakly perturbed. Increasing the mixing ratio to 1:1 (N₂O:H₂O) produces a prominent dangling O–H feature at 3652 cm⁻¹ (Figure S5). A weaker hump at 3491 cm⁻¹ is also observed, attributable to N₂O–H₂O interactions, although its specific origin remains unclear. Upon warming to 100 K, both peaks vanish, indicating compaction of the ice matrix and reduced N₂O content. These experiments show that N₂O CH does not form spontaneously from an N₂O–H₂O ice mixture under UHV conditions. Consequently, we focused on the formation of sI ETO CH, which was later used as a promoter for N₂O CH formation.

To begin, pure ETO ice was investigated under UHV conditions. Figure 2a shows the temperature-dependent RAIR spectra of ETO in the ring-breathing region (ν_3). At 10 K, vapor-deposited ETO formed an amorphous ice, evident from a broad peak centered at 1269 cm⁻¹. Upon annealing to 90 K, crystallization occurred, as indicated by the emergence of a sharp peak at 1267 cm⁻¹.⁴⁶ In the CH₂ bending region, the initially broad band sharpens and resolves into two peaks at 1466 and 1460 cm⁻¹ (Figure S6a). Upon further warming to 120 K, ETO completely desorbs from the surface.

To study the formation of ETO CH, approximately 300 ML of ETO–H₂O (1:5) vapor mixture was codeposited and annealed to 130 K (Figure 2b). It is well-established that ETO forms sI CH under both high-pressure and vacuum conditions, and its characteristic RAIR spectra are also well-documented.^{47–52} In particular, the ring-breathing mode of ETO in sI CHs typically exhibits a doublet with a 2 cm⁻¹ splitting, attributed to ETO molecules occupying large cages in two distinct orientations.⁴⁸ A smaller hump, ~13 cm⁻¹ blue-shifted from the main peak, has been assigned to ETO trapped in smaller cages.⁴⁸ Although this splitting is not always fully resolved at elevated temperatures, it becomes clearer at lower temperatures due to reduced thermal broadening.^{48,51}

In our experiment, after annealing to 130 K, we observed a broadened peak with a small shoulder at around 1276 cm⁻¹ (Figure 2b), suggesting the formation of clathrate structures. Upon cooling the sample back down to 10 K, a clearer spectral splitting emerged with increased peak intensity, indicative of more ordered structural arrangements. Deconvolution of the spectrum revealed two sharp peaks at 1268 cm⁻¹ and 1266 cm⁻¹, along with a smaller intensity feature at 1276 cm⁻¹ (Figure 2b). This splitting is possible due to the different orientation of ETO inside sI large cages.⁴⁷ The peak positions are consistent with those in earlier reports. Bertie and Othen⁴⁸ observed features at 1268 and 1270 cm⁻¹, while Fleyfel and Devlin⁴⁷ reported 1266 and 1268 cm⁻¹ for ETO in a 5¹²6² cage. Taken together, these observations suggest the facile formation of ETO CH from the amorphous ice mixture at 130 K. In the CH₂ bending region (Figure S6b), no definitive changes were observed due to very low intensity. Concurrently, crystallization of amorphous solid water (ASW) was evident, as indicated by the sharpening of features in the O–H stretching region (Figure S7). While ETO CH formation under vacuum has been previously reported,^{48,53} its formation from in ASW under UHV conditions has not been demonstrated. One motivation for studying ETO CH in this manner is to examine

whether the surface of ETO CH can facilitate the nucleation of N₂O CH.

In the first attempt, we failed to create N₂O CH by thermal annealing the N₂O–H₂O ice mixture. Later, we took a N₂O–H₂O ice mixture on top of ETO ice and, through thermal annealing, created a mixture of ETO–N₂O–H₂O ice at 130 K (Figure 3). When ETO started to form sI CH, a clear splitting was observed in the N–N–O asymmetric stretching region. The peak at 2227 cm⁻¹ was split to make a new peak at 2220 cm⁻¹, and a small hump was observed at 2233 cm⁻¹. The peak intensity at 2233 cm⁻¹ decreases relatively slowly (and remains nearly constant over 120–180 min), compared to the peak intensity of 2227 cm⁻¹ (Figure 3). This behavior indicates two N₂O populations, with the persistent component stabilized in well-defined sites consistent with N₂O trapped in CH cages, whereas the faster-decreasing band reflects more weakly bound ASW-trapped N₂O that desorbs. The area under the two peaks (at 2233 cm⁻¹ and 2220 cm⁻¹) gave a ratio of 1:4.5, which is close to the population distribution in the small and large cages of sI CH. In the symmetric stretching region (Figure S8) two new peaks were observed at 1282 and 1292 cm⁻¹. It is worth noting that peak deconvolution can not be done for symmetric stretch due to a poor signal-to-noise ratio. Additionally, in the ring-breathing mode of ETO, a broadened peak at 1269 cm⁻¹ and a small hump at 1276 cm⁻¹ (Figure 3) were observed, consistent with previous observations of pure ETO sI CH.⁴⁸ A Raman spectroscopic study reported by Yang et al.⁵⁴ shows the difference between the large cage and small cage peak is 13 cm⁻¹ (for asymmetric stretch) and 8 cm⁻¹ (for symmetric stretch), respectively, which closely match with the current IR study. This proves the formation of sI N₂O CH in the presence of ETO CH.

The nucleation behavior of CH from N₂O is notably complex. In the absence of ETO, prolonged thermal annealing over several hours failed to induce CH formation; instead, the ASW began to crystallize. This observation clearly indicates that the homogeneous nucleation of CH from an amorphous N₂O:H₂O ice mixture is not feasible without the presence of a third component. However, once the sI CH formation of ETO commenced in the ETO–N₂O–H₂O ice mixture, CH formation from N₂O was also observed. Two possible nucleation pathways can be considered: (i) simultaneous nucleation of ETO and N₂O hydrates due to their homogeneous distribution in the ice matrix, or (ii) heterogeneous nucleation of N₂O hydrate on the surface of the preformed ETO hydrate. Given the limited experimental technique, it remains challenging to distinguish between these mechanisms or to rule out the possibility that both are occurring concurrently.

To support the IR results, we carried out gas-phase DFT calculations for N₂O and ETO in sI and sII CH cages. The optimized geometries of the empty 5¹², 5¹²6², and 5¹²6⁴ CH cages, as well as those containing ETO and N₂O, are shown in Figure 4. The vibrational frequencies of the isolated ethylene oxide and nitrous oxide molecules, along with their frequencies when confined within the three different cages, are shown in Table 1. Free N₂O exhibits an asymmetric stretch at 2267.93 cm⁻¹, consistent with a prior report,⁵⁵ and ETO shows ring breathing mode at 1257.19 cm⁻¹. When these molecules are confined within the smaller 5¹² CH cage, they exhibit blue shifts of 18.76 cm⁻¹ and 15 cm⁻¹ for N₂O and ETO, respectively. However, when placed inside the comparatively larger 5¹²6² and 5¹²6⁴ CH cages, the N₂O molecule shows

lower blue shifts of 4.96 cm^{-1} and 1.81 cm^{-1} , while the ETO molecule exhibits blue shifts of 5.51 cm^{-1} and 1.98 cm^{-1} , respectively. The molecules exhibit a stronger blue shift when confined within smaller cages due to steric restrictions that distort molecular bonds and elevate vibrational frequencies. In contrast, larger cages provide greater spatial freedom and structural flexibility, minimizing steric effects and resulting in only slight changes in vibrational modes.⁵⁶ It is important to note that no chemical bond formation was observed between the water molecules of the CH cages and guest molecules (N_2O and ETO). Though we observed distortion of the CH cages, we did not observe cage breakage while guest molecules were confined in them. Hydrogen bonding between the oxygen and hydrogen molecules forming the CH cages and weak interaction between the cage and guest molecules provide the stability to molecule-confined CH cages.⁵⁷

To further prove the heterogeneous nucleation of N_2O CH in amorphous ice, we have used two stable sII CH former molecules, DME and THF (Figure 5).⁵⁸ Both of the molecules are known to form sII large cage CH in UHV under cryogenic conditions. We deposited sequentially THF/DME and $\text{H}_2\text{O} + \text{N}_2\text{O}$ ice mixture at 10 K and annealed the sample at 130 K for a few hours. Figure 5 shows IR spectra of $\text{DME}@(\text{H}_2\text{O}+\text{N}_2\text{O})$ (Figure 5a) and $\text{THF}@(\text{H}_2\text{O}+\text{N}_2\text{O})$ (Figure 5b) ice mixture in the N–N–O and C–O asymmetric stretch. Previous studies showed that THF and DME form sII CH where the $5^{12}6^4$ cage is occupied by the THF and DME with a distinct assigned IR peak 1074 cm^{-1} and 1096 cm^{-1} .^{22,53,59} The peaks at 1090 cm^{-1} and $1033/1054\text{ cm}^{-1}$ are attributed to DME and THF molecules trapped within ASW. In this system, during the formation of THF/DME CHs in the N–N–O asymmetric stretching region a new peak arises at 2220 cm^{-1} , which can be assigned to the large cages. Interestingly, we have not observed any peak around 2233 cm^{-1} , which indicates the absence of small cages. Here, it is difficult to assign whether this assignment occurs due to the large cages of sI or sII. It is worth noting that N_2O is not going to preexisting vacant small cages created by THF/DME. These additional experiments demonstrate that, without any incubation time at 130 K, N_2O can spontaneously form a CH only in the presence of supporting guest molecules such as ETO, DME, or THF, which facilitate nucleation.

In conclusion, we have demonstrated the formation of N_2O and ETO CHs under UHV and cryogenic conditions. While the formation of ETO CHs in high vacuum was previously reported by the Devlin group,^{28,58} to the best of our knowledge, this is the first report of ETO CH formation under such conditions. Notably, we also present the first IR spectra of N_2O CHs. A key conclusion from this study is that homogeneous nucleation of N_2O CH does not occur readily from an amorphous N_2O – H_2O ice mixture, even upon annealing to 130 K. However, when codeposited with a secondary guest molecule known to spontaneously form clathrates, such as ETO, DME, or THF, N_2O readily forms CHs upon annealing. In the presence of ETO, N_2O forms sI CHs, while in the presence of DME or THF, N_2O appears to occupy larger cages; however, due to limited spectroscopic evidence, we could not conclusively assign these to either sI or sII CHs. To support our experimental observations, DFT calculations were performed for free and encaged N_2O and ETO molecules within 5^{12} , $5^{12}6^2$, and $5^{12}6^4$ cages. The calculated IR spectra indicate that molecules confined in

smaller cages experience greater steric hindrance, resulting in larger blue shifts compared to those in larger cages.

■ ASSOCIATED CONTENT

Supporting Information

The Supporting Information is available free of charge at <https://pubs.acs.org/doi/10.1021/acs.jpcllett.5c02778>.

Experimental section (including experimental setup, materials and reagents, and sample preparation) and temperature and time-dependent RAIR spectra (PDF)
Transparent Peer Review report available (PDF)

■ AUTHOR INFORMATION

Corresponding Authors

Sharma S. R. K. C. Yamijala – Department of Chemistry, Indian Institute of Technology Madras, Chennai 600036, India; orcid.org/0000-0003-1773-9226; Email: yamijala@iitm.ac.in

Rajnish Kumar – International Centre for Clean Water, IIT Madras Research Park, Chennai 600113, India; Department of Chemical Engineering and School of Sustainability, Indian Institute of Technology Madras, Chennai 600036, India; orcid.org/0000-0002-4172-2638; Email: rajnish@iitm.ac.in

Thalappil Pradeep – DST Unit of Nanoscience (DST UNS) and Thematic Unit of Excellence (TUE), Department of Chemistry, Indian Institute of Technology Madras, Chennai 600036, India; International Centre for Clean Water, IIT Madras Research Park, Chennai 600113, India; orcid.org/0000-0003-3174-534X; Email: pradeep@iitm.ac.in

Authors

Bijesh K. Malla – DST Unit of Nanoscience (DST UNS) and Thematic Unit of Excellence (TUE), Department of Chemistry, Indian Institute of Technology Madras, Chennai 600036, India; Department of Chemical Engineering, Indian Institute of Technology Madras, Chennai 600036, India; orcid.org/0009-0005-1148-0884

Soham Chowdhury – DST Unit of Nanoscience (DST UNS) and Thematic Unit of Excellence (TUE), Department of Chemistry, Indian Institute of Technology Madras, Chennai 600036, India

Samir Kumar Nayak – Department of Chemistry, Indian Institute of Technology Madras, Chennai 600036, India

Sofia Sara Baji – Department of Chemistry, Mar Ivanios College, Thiruvananthapuram, Kerala 695015, India

Teena J Mathew – Department of Chemistry, Mar Ivanios College, Thiruvananthapuram, Kerala 695015, India

Rabin Rajan J Methikkalam – Department of Chemistry, Mar Ivanios College, Thiruvananthapuram, Kerala 695015, India

Complete contact information is available at: <https://pubs.acs.org/doi/10.1021/acs.jpcllett.5c02778>

Author Contributions

[‡]B.K.M. and S.C. contributed equally. B.K.M. designed the experiments. B.K.M., S.C., S.S.B., and T.J.M. performed the experiments. B.K.M. and S.C. analyzed the results. T.P. and R.K. supervised the progress. S.K.N. and S.S.R.K.C.Y. performed the quantum chemical calculations. B.K.M. wrote the first draft of the manuscript. The final version of the manuscript was prepared with the contributions of all authors.

Notes

The authors declare no competing financial interest.

ACKNOWLEDGMENTS

We acknowledge the Science and Engineering Research Board (SERB), Department of Science and Technology (DST), and Government of India for research funding. T.P. acknowledges funding from the Centre of Excellence (CoE) on Molecular Materials and Functions under the Institution of Eminence scheme of IIT Madras. S.S.R.K.C.Y. acknowledges the financial support of IIT Madras through the Mphasis faculty fellowship and its new faculty support grants NFSG (IP2021/0972CY/NFSC008973), NFIG (RF2021/0577CY/NFIG008973), and Anusandhan National Research Foundation (ANRF). S.C. thanks IITM for their research fellowship. S.K.N. thanks the Prime Minister's Research Fellowship (PMRF) for his research fellowship.

REFERENCES

- (1) Griffis, T. J.; Chen, Z.; Baker, J. M.; Wood, J. D.; Millet, D. B.; Lee, X.; Venterea, R. T.; Turner, P. A. Nitrous Oxide Emissions Are Enhanced in a Warmer and Wetter World. *Proc. Natl. Acad. Sci. U. S. A.* **2017**, *114* (45), 12081–12085.
- (2) Portmann, R. W.; Daniel, J. S.; Ravishankara, A. R. Stratospheric Ozone Depletion Due to Nitrous Oxide: Influences of Other Gases. *Philos. Trans. R. Soc. B Biol. Sci.* **2012**, *367* (1593), 1256–1264.
- (3) *Climate Change 2022 - Mitigation of Climate Change*; Intergovernmental Panel on Climate Change (IPCC), Ed.; Cambridge University Press, 2023.
- (4) Ziurys, L. M.; Apponi, A. J.; Hollis, J. M.; Snyder, L. E. Detection of Interstellar N₂O: A New Molecule Containing an N-O Bond. *Astrophys. J.* **1994**, *436*, L181.
- (5) Halfen, D. T.; Apponi, A. J.; Ziurys, L. M. Evaluating the N/O Chemical Network: The Distribution of N₂O and NO in the Sagittarius B2 Complex. *Astrophys. J.* **2001**, *561* (1), 244–253.
- (6) Nazari, P.; Rocha, W. R. M.; Rubinstein, A. E.; Slavcinska, K.; Rachid, M. G.; Van Dishoeck, E. F.; Megeath, S. T.; Gutermuth, R.; Tyagi, H.; Brunken, N.; et al. Hunting for Complex Cyanides in Protostellar Ices with the JWST - A Tentative Detection of CH₃CN and C₂H₅CN. *Astron. Astrophys.* **2024**, *686*, A71.
- (7) Sloan, E. D., Jr.; Koh, C. A.; Koh, C. A. *Clathrate Hydrates of Natural Gases*; CRC Press, 2007.
- (8) Sloan, E. D. Fundamental Principles and Applications of Natural Gas Hydrates. *Nature*; Nature Publishing Group November 20, 2003; pp 353–359.
- (9) Sloan, E. D. J.; Koh, C. A. Hydrates in the Earth. *Clathrate Hydrates of Natural Gases* **2007**, 20074156, 537–642.
- (10) Sloan, E. D. J.; Koh, C. A. Introduction: Clathrate Hydrates of Natural Gases. *Clathrate Hydrates Nat. Gases* **2008**, I–XXV.
- (11) Luspay-Kuti, A.; Mousis, O.; Hässig, M.; Fuselier, S. A.; Lunine, J. I.; Marty, B.; Mandt, K. E.; Wurz, P.; Rubin, M. The Presence of Clathrates in Comet 67P/Churyumov-Gerasimenko. *Sci. Adv.* **2016**, *2* (4), No. e1501781.
- (12) Ghosh, J.; Vishwakarma, G.; Kumar, R.; Pradeep, T. Formation and Transformation of Clathrate Hydrates under Interstellar Conditions. *Acc. Chem. Res.* **2023**, *56* (16), 2241–2252.
- (13) Malla, B. K.; Vishwakarma, G.; Chowdhury, S.; Selvarajan, P.; Pradeep, T. Formation of Ethane Clathrate Hydrate in Ultrahigh Vacuum by Thermal Annealing. *J. Phys. Chem. C* **2022**, *126* (42), 17983–17989.
- (14) Tychengulova, A.; Katpayeva, K.; Shomsheva, S.; Ibragimova, S.; Golikov, O.; Yerezhep, D.; Sokolov, D.; Aldiyarov, A. Laboratory Studies of the Clathrate Hydrate Formation in the Carbon Dioxide-Water Mixtures at Interstellar Conditions. *ACS Omega* **2025**, *10* (1), 1237–1248.
- (15) Malla, B. K.; Yang, D.-S.; Pradeep, T. Growth of Clathrate Hydrates in Nanoscale Ice Films Observed Using Electron Diffraction and Infrared Spectroscopy. *J. Phys. Chem. Lett.* **2025**, *16* (1), 365–371.
- (16) Khurana, M.; Yin, Z.; Linga, P. A Review of Clathrate Hydrate Nucleation. *ACS Sustain. Chem. Eng.* **2017**, *5* (12), 11176–11203.
- (17) Guo, G.-J.; Zhang, Z. Open Questions on Methane Hydrate Nucleation. *Commun. Chem.* **2021**, *4* (1), 102.
- (18) Jacobson, L. C.; Molinero, V. Can Amorphous Nuclei Grow Crystalline Clathrates? The Size and Crystallinity of Critical Clathrate Nuclei. *J. Am. Chem. Soc.* **2011**, *133* (16), 6458–6463.
- (19) Malla, B. K.; Chowdhury, S.; Vishwakarma, G.; Kumar, R.; Pradeep, T. Dissociation and Reformation of CO₂ Clathrate Hydrate Cages in Amorphous Ice Thin Film under Ultrahigh Vacuum. *J. Phys. Chem. Lett.* **2025**, *16* (20), 4982–4989.
- (20) Chowdhury, S.; Malla, B. K.; Vishwakarma, G.; Nyayban, A.; Pradeep, T. Composition-Dependent Formation and Dissociation of Structure I and Structure II Clathrate Hydrates of Trimethylene Oxide in Ultrahigh Vacuum. *J. Phys. Chem. C* **2025**, *129* (19), 8937–8945.
- (21) Vishwakarma, G.; Malla, B. K.; Chowdhury, S.; Khandare, S. P.; Pradeep, T. Existence of Acetaldehyde Clathrate Hydrate and Its Dissociation Leading to Cubic Ice under Ultrahigh Vacuum and Cryogenic Conditions. *J. Phys. Chem. Lett.* **2023**, *14* (23), 5328–5334.
- (22) Malla, B. K.; Vishwakarma, G.; Chowdhury, S.; Nayak, S. K.; Yamijala, S. S. R. K. C.; Pradeep, T. Formation and Dissociation of Dimethyl Ether Clathrate Hydrate in Interstellar Ice Mimics. *J. Phys. Chem. C* **2024**, *128* (6), 2463–2470.
- (23) Ghosh, J.; Bhuin, R. G.; Ragupathy, G.; Pradeep, T. Spontaneous Formation of Tetrahydrofuran Hydrate in Ultrahigh Vacuum. *J. Phys. Chem. C* **2019**, *123* (26), 16300–16307.
- (24) Sugahara, T.; Kawazoe, A.; Sugahara, K.; Ohgaki, K. High-Pressure Phase Equilibrium and Raman Spectroscopic Studies on the Nitrous Oxide Hydrate System. *J. Chem. Eng. Data* **2009**, *54* (8), 2301–2303.
- (25) Takeya, S.; Hachikubo, A. Crystal Structure and Guest Distribution of N₂O Hydrate Determined by Powder X-Ray Diffraction Measurements. *Cryst. Growth Des.* **2022**, *22* (2), 1345–1351.
- (26) Sun, N.; Li, Y.; Qiu, N.; Du, S. Ab Initio Studies of Structural and Mechanical Properties of NH₃, NO, and N₂O Hydrates. *ACS Omega* **2023**, *8* (24), 22018–22025.
- (27) Tse, J. S.; McKinnon, W. R.; Marchi, M. Thermal Expansion of Structure I Ethylene Oxide Hydrate. *J. Phys. Chem.* **1987**, *91* (15), 4188–4193.
- (28) Maşlakçı, Z.; Devlin, J. P.; Uras-Aytemiz, N. H-Bonding Behavior of Ethylene Oxide within the Clathrate Hydrates Revisited: Experiment and Theory. *Chem. Phys. Lett.* **2020**, *754* (May), 137728.
- (29) Bauer, R. P. C.; Ravichandran, A.; Tse, J. S.; Appathurai, N.; King, G.; Moreno, B.; Desgreniers, S.; Sammynaiken, R. In Situ X-Ray Diffraction Study on Hydrate Formation at Low Temperature in a High Vacuum. *J. Phys. Chem. C* **2021**, *125* (48), 26892–26900.
- (30) Zang, X.; Ueno, Y.; Kitadai, N. Photochemical Synthesis of Ammonia and Amino Acids from Nitrous Oxide. *Astrobiology* **2022**, *22* (4), 387–398.
- (31) Bag, S.; Bhuin, R. G.; Methikkalam, R. R. J.; Pradeep, T.; Kephart, L.; Walker, J.; Kuchta, K.; Martin, D.; Wei, J. Development of Ultralow Energy (1–10 eV) Ion Scattering Spectrometry Coupled with Reflection Absorption Infrared Spectroscopy and Temperature Programmed Desorption for the Investigation of Molecular Solids. *Rev. Sci. Instrum.* **2014**, *85* (1), 014103.
- (32) Becke, A. D. Density-functional Thermochemistry. III. The Role of Exact Exchange. *J. Chem. Phys.* **1993**, *98* (7), 5648–5652.
- (33) Krishnan, R.; Binkley, J. S.; Seeger, R.; Pople, J. A. Self-consistent Molecular Orbital Methods. XX. A Basis Set for Correlated Wave Functions. *J. Chem. Phys.* **1980**, *72* (1), 650–654.
- (34) Laane, J.; Ohlsen, J. R. Characterization of Nitrogen Oxides by Vibrational Spectroscopy. *Prog. Inorg. Chem.* **1980**, *27*, 465–513.
- (35) Gimmler, G.; Havenith, M. High-Resolution IR Spectroscopy of the N₂O-H₂O and N₂O-D₂O van Der Waals Complexes. *J. Mol. Spectrosc.* **2002**, *216* (2), 315–321.

- (36) Kumi, G.; Malyk, S.; Hawkins, S.; Reisler, H.; Wittig, C. Amorphous Solid Water Films: Transport and Guest-Host Interactions with CO₂ and N₂O Dopants. *J. Phys. Chem. A* **2006**, *110* (6), 2097–2105.
- (37) Hudson, R. L.; Loeffler, M. J.; Gerakines, P. A. Infrared Spectra and Band Strengths of Amorphous and Crystalline N₂O. *J. Chem. Phys.* **2017**, *146* (2), 24304.
- (38) Elisabetta Palumbo, M.; Baratta, G. A.; Collings, M. P.; McCoustra, M. R. S. The Profile of the 2140 Cm⁻¹ Solid CO Band on Different Substrates. *Phys. Chem. Chem. Phys.* **2006**, *8* (2), 279–284.
- (39) Cassidy, A.; Jørgensen, M. R. V.; Rosu-Finsen, A.; Lasne, J.; Jørgensen, J. H.; Glavic, A.; Lauter, V.; Iversen, B. B.; McCoustra, M. R. S.; Field, D. Dipole-Oriented Molecular Solids Can Undergo a Phase Change and Still Maintain Electrical Polarization. *J. Phys. Chem. C* **2016**, *120* (42), 24130–24136.
- (40) Cardini, G.; Signorini, G. F.; Salvi, P. R.; Righini, R. Molecular Dynamics and Head-Tail Disorder in the Raman Spectrum of Crystalline N₂O. *Chem. Phys. Lett.* **1987**, *142* (6), 570–574.
- (41) Mills, R. L.; Olinger, B.; Cromer, D. T.; LeSar, R. Crystal Structures of N₂O to 12 GPa by X-ray Diffraction. *J. Chem. Phys.* **1991**, *95* (7), 5392–5398.
- (42) Balog, R.; Cicman, P.; Jones, N. C.; Field, D. Spontaneous Dipole Alignment in Films of N₂O. *Phys. Rev. Lett.* **2009**, *102* (7), 073003.
- (43) Mifsud, D. V.; Hailey, P. A.; Herczku, P.; Sulik, B.; Juhász, Z.; Kovács, S. T. S.; Kaňuchová, Z.; Ioppolo, S.; McCullough, R. W.; Paripás, B.; Mason, N. J. Comparative Electron Irradiations of Amorphous and Crystalline Astrophysical Ice Analogues. *Phys. Chem. Chem. Phys.* **2022**, *24* (18), 10974–10984.
- (44) Malla, B. K.; Chowdhury, S.; Paliwal, D.; K. M., H.; Vishwakarma, G.; Methikkalam, R. R. J.; Pradeep, T. Simulated Interstellar Photolysis of N₂O Ice: Selectivity in Photoproducts. *J. Phys. Chem. C* **2025**, *129* (2), 1120–1128.
- (45) Smith, R. S.; Matthiesen, J.; Knox, J.; Kay, B. D. Crystallization Kinetics and Excess Free Energy of H₂O and D₂O Nanoscale Films of Amorphous Solid Water. *J. Phys. Chem. A* **2011**, *115* (23), 5908–5917.
- (46) Hudson, R. L.; Gerakines, P. A.; Yarnall, Y. Y. Infrared Spectra and Optical Constants of Astronomical Ices: V. Cyclopropane and Ethylene Oxide. *Icarus* **2023**, *396*, 115499.
- (47) Fleyfel, F.; Devlin, J. P. FT-IR Spectra of 90 K Films of Simple, Mixed, and Double Clathrate Hydrates of Trimethylene Oxide, Methyl Chloride, Carbon Dioxide, Tetrahydrofuran, and Ethylene Oxide Containing Decoupled D₂O. *J. Phys. Chem.* **1988**, *92* (3), 631–635.
- (48) Bertie, J. E.; Othen, D. A. The Infrared Spectrum of Ethylene Oxide Clathrate Hydrate at 100°K between 4000 and 360 Cm⁻¹. *Can. J. Chem.* **1973**, *51* (8), 1159–1168.
- (49) Yang, X.; Du, S.; Hao, Y.; Xu, J. Molecular Dynamics Simulation of Promoting Nucleation of CO₂ Hydrate by Ethylene Oxide and Tetrahydrofuran. *IOP Conf. Ser. Earth Environ. Sci.* **2021**, *675* (1), 012183.
- (50) Fleyfel, F.; Devlin, J. P. Carbon Dioxide Clathrate Hydrate Epitaxial Growth: Spectroscopic Evidence for Formation of the Simple Type-II CO₂ Hydrate. *J. Phys. Chem.* **1991**, *95* (9), 3811–3815.
- (51) Cwiklik, L.; Devlin, J. P. Hindering of Rotational Motion of Guest Molecules in the Type I Clathrate Hydrate. *Chem. Phys. Lett.* **2010**, *494* (4–6), 206–212.
- (52) Williams, K. D.; Devlin, J. P. Formation and Spectra of Clathrate Hydrates of Methanol and Methanol-Ether Mixtures. *J. Mol. Struct.* **1997**, *416* (1–3), 277–286.
- (53) Richardson, H. H.; Wooldridge, P. J.; Devlin, J. P. FT-IR Spectra of Vacuum Deposited Clathrate Hydrates of Oxirane H₂S, THF, and Ethane. *J. Chem. Phys.* **1985**, *83* (9), 4387.
- (54) Yang, Y.; Shin, D.; Choi, S.; Lee, J. W.; Cha, M.; Kim, D.; Yoon, J. H. Cage Occupancy and Stability of N₂O-Encaged Structure I and II Clathrate Hydrates. *Energy Fuels* **2016**, *30* (11), 9628–9634.
- (55) Zúñiga, J.; Bastida, A.; Requena, A. Theoretical Calculations of Vibrational Frequencies and Rotational Constants of the N₂O Isotopomers. *J. Mol. Spectrosc.* **2003**, *217* (1), 43–58.
- (56) Ramamurthy, A.; Baburao, G.; Jahnvi, A.; Ragupathy, G. Encapsulation of Greenhouse Gases in Clathrate Hydrates with Insights into Structure, Energetics, Chemical Interactions, and Environmental Implications. *Sci. Rep.* **2025**, *15* (1), 24090.
- (57) Ramya, K. R.; Pavan Kumar, G. V.; Venkatnathan, A. Raman Spectra of Vibrational and Librational Modes in Methane Clathrate Hydrates Using Density Functional Theory. *J. Chem. Phys.* **2012**, *136* (17), 174305.
- (58) Buch, V.; Devlin, J. P.; Monreal, I. A.; Jagoda-Cwiklik, B.; Uras-Aytemiz, N.; Cwiklik, L. Clathrate Hydrates with Hydrogen-Bonding Guests. *Phys. Chem. Chem. Phys.* **2009**, *11* (44), 10245–10265.
- (59) Peeters, Z.; Rodgers, S. D.; Charnley, S. B.; Schriver-Mazzuoli, L.; Schriver, A.; Keane, J. V.; Ehrenfreund, P. Astrophysics Astrochemistry of Dimethyl Ether. *A&A* **2006**, *445*, 197–204.